How to Cite: Abdulsattar, M.A. (2025). WO_3 Doped SnS_2 Gas Sensor Response to NO_2: Effect of Temperature and Humidity Using Transition State Theory Formalism. *Eurasian Journal of Chemistry, 30, 4(120), 34–44.* https://doi.org/10.31489/2959-0663/4-25-5

PHYSICAL AND ANALYTICAL CHEMISTRY

Article

Received: 8 July 2025 | Revised: 29 October 2025 |
Accepted: 3 November 2025 | Published online: 15 November 2025

UDC 544.4, 544.18

https://doi.org/10.31489/2959-0663/4-25-5

Mudar A. Abdulsattar

Ministry of Science and Technology, Baghdad, Iraq
*(*Author's e-mail: mudarahmed3@yahoo.com)*

WO_3 Doped SnS_2 Gas Sensor Response to NO_2: Effect of Temperature and Humidity Using Transition State Theory Formalism

Several factors frequently affect gas sensors, including sensing material, doping, temperature, detected gas properties, humidity, manufacturing method, etc. The present work studies WO_3 doped SnS_2 gas sensor response to NO_2, considering the above factors using transition state theory formalism. The reaction rate equation in transition state theory was used to estimate the change in the number of vacancies in a 30 % WO_3-doped SnS_2 sensor when NO_2 gas passed over its surface. Temperature dependence of Gibbs energy of adsorption and transition was evaluated at the effective temperatures. Effective temperatures were the temperatures after which NO_2 gas dissociates and can no longer be detected. The effect of temperature and humidity was evaluated using logistic functions. Response, response time, and NO_2 concentration were calculated and compared with the experiment. Interestingly, the lowest Gibbs energy of transition as a function of 30 % WO_3 doping percentage was very close to the highest experimental response. WO_3 doped SnS_2 gas sensor is stable for an extended period, as proved experimentally and theoretically. Transition state theory enabled the calculation of changes in the number of vacancies and various experimentally obtained quantities that cannot be evaluated using density functional theory alone.

Keywords: WO_3 Doped SnS_2, NO_2 gas sensor, Density functional theory, Transition state theory, effecting temperature, doping, response time, Gibbs energy

Introduction

Tin disulfide (SnS_2) is a semiconductor similar to SnO_2 in several properties. SnS_2 is used in gas sensors and mosaic work. Pyramids are observed on the SnS_2 surface [1]. Pyramid shapes increase the gas sensitivity by increasing the surface area of the gas sensor. SnS_2 detects several gases, including NH_3, NO_2, H_2S, etc. [2–4].

Tungsten trioxide (WO_3) is one of the oxides with the highest number of oxygen atoms. Having a large number of oxygen atoms is beneficial in gas sensors since it can be used to exchange oxygen atoms with the detected gas. WO_3 gas sensors detect several gases, such as H_2S, NO_2, and H_2 [5–7].

Nitrogen dioxide (NO_2) is one of several other nitrogen oxides. This oxide is poisonous for humans if its concentration becomes higher than a permissible concentration. The allowed NO_2 concentration is 1–5 ppm [8]. As a result, the NO_2 gas detector should detect NO_2 concentrations higher than one (1) ppm. The highest response of NO_2 sensors is close to its dissociation temperature but can also be detected at room temperature [9].

Density functional theory (DFT) is the usual method used in gas sensor simulation procedures [10]. However, the simulation results are limited and cannot be compared to the findings of the experimental results, such as response, response time, and effect of temperature or humidity if only DFT is used. Recently, methods that depend on reaction rate theories, such as the Arrhenius equation, collision theory, or transition state theory, have been developed to account for these deficiencies [11–13]. Transition state theory (TST) is

more sophisticated and advanced than older collision theory and the Arrhenius equation. Transition state theory relates activation energy with Gibbs free energy of transition, a valid thermodynamic quantity that is more investigated to solve current applications [12, 13].

Many materials were used previously to detect NO_2 gas. These materials include SnO_2 [14], ZnO [15], WO_3 [16] etc. In most cases, doping increases the sensitivity of material toward gases, which is also the case with NO_2 sensors. Mathematically, doping increases the entropy of a material and reduces Gibbs free energy of transition or activation value for better detection, as shall be clear in the present work. Vacancies have significant roles in gas sensing. For reducing gases such as H_2, CH_4, H_2S, etc., vacancies increase as the sensor material is exposed to the detected gas. In oxidizing gases such as present NO_2 gas, vacancies decrease as the detected gas passes over the detecting material.

The present work calculates WO_3 doped SnS_2 gas sensor response to NO_2 using transition state theory formalism. Gibbs free energy of transition is calculated at different doping percentages using pristine and WO_3-doped SnS_2 clusters. Reaction rates are used to evaluate the change in the number of vacancies with appropriate parameters considering previous calculations of different gases. Response and response time are evaluated from the reaction rate and compared with experimental values as a function of temperature. Humidity and NO_2 gas properties' effects as a function of temperature are considered using a logistic function. The stability of the sensor with time is compared with the experiment. The impact of gas properties, temperature, and humidity cannot be evaluated using the DFT method alone, which is the main reason for using TST.

Computation Details

The Gaussian 09 molecular modeling program performed present DFT calculations [17]. Heavy atoms such as Sn and W cannot be described using the same basis set for light elements such as O, N, and S as a Gaussian program input. As a result, B3LYP/6-311G** is used to describe light atoms, while Sn and W are described using SDD basis sets (Stuttgart/Dresden). Dispersion corrections are essential in gas sensor calculations since long-range interactions are inevitable. Dispersion corrections are added via the GD3BJ method in the Gaussian 09 program.

NO_2 gas is known to decompose at temperatures around 200℃ as in the equation [18]:

$$NO_2 \rightarrow NO + ½O_2 \ (\Delta G = 0.319 \text{ eV}), \quad (1)$$

ΔG stands for the difference in Gibbs energy between reaction products and reaction reactants. The value of the Gibb free energy (ΔG) of this endergonic reaction (positive value of (ΔG)) can be supplied at temperatures around 200 °C by the thermal energy of the collision of two NO_2 molecules [19]. As a result, many gas sensors prefer temperatures around 200 °C to detect NO_2 gas [20, 21]. In fact, detecting NO_2 at temperatures extremely higher than 200 °C becomes more difficult as the temperature increases.

SnS_2 compound reacts with NO_2 gas at the surface pyramid structures [22]. SnS_2 surface pyramid structures are similar to SnO_2, with many vacancies [23]. The largest possible size cluster that can be handled by theoretical calculations is used. The stable pyramid cluster with ten Sn atoms is $Sn_{10}S_{16}$ [19]. The stable $Sn_{10}S_{16}$ cluster is in equilibrium with a smaller number of $Sn_{10}S_{15}$ (with sulfur vacancy) and $Sn_{10}S_{17}$ (over sulfurized) clusters depending on the energy required to remove or add S atoms to the stable $Sn_{10}S_{16}$ cluster [19]. The stable cluster $Sn_{10}S_{16}$ cannot react with NO_2 gas or be further oxidized by oxygen as in the equations (The values of ΔG are at standard pressure and temperature (25 °C and 1 bar) unless mentioned otherwise):

$$Sn_{10}S_{16} + NO_2 \rightarrow Sn_{10}S_{16}O + NO \ (\Delta G = 1.966 \text{ eV}), \quad (2)$$

$$Sn_{10}S_{16} + ½O_2 \rightarrow Sn_{10}S_{16}O \ (\Delta G = 1.531 \text{ eV}). \quad (3)$$

The high values of endergonic reactions make these reactions unfavorable reactions. However, NO_2 can still be adsorbed (by van der Waals interaction) by the $Sn_{10}S_{16}$ cluster as in the reaction:

$$Sn_{10}S_{16} + NO_2 \rightarrow [Sn_{10}S_{16} \text{ --- } NO_2]^a \ (\Delta G = 0.133 \text{ eV}). \quad (4)$$

In Eq. (4), $[Sn_{10}S_{16} \text{ --- } NO_2]^a$ represents the adsorption state. Although the Gibbs free energy of the reaction is positive in the above equation, the small value of ΔG can be supplied by the thermal energies of colliding particles. Only the $Sn_{10}S_{15}$ cluster (with sulfur vacancy) can be oxidized by NO_2 gas (exergonic reaction) as in the equation:

$$Sn_{10}S_{15} + NO_2 \rightarrow Sn_{10}S_{15}O + NO \ (\Delta G = -0.717 \text{ eV}). \quad (5)$$

On the other hand, the reaction of the $Sn_{10}S_{15}$ cluster with adsorbed NO_2 gas is more energetically favorable, as in the equation:

$$[Sn_{10}S_{16}\text{ --- }NO_2]^a + Sn_{10}S_{15} \rightarrow Sn_{10}S_{16} + Sn_{10}S_{15}O + NO\ (\Delta G = -0.868\ \text{eV}). \quad (6)$$

After doping SnS_2 with WO_3, the reaction of NO_2 gas with the doped clusters takes another trend. The nearest cluster to the available experimental doping is the $W_2Sn_8S_{10}O_8$ cluster. The $W_2Sn_8S_{10}O_8$ cluster is stable in an oxygen environment, i.e., the removing or adding oxygen atoms to the cluster is endergonic as in the equations:

$$W_2Sn_8S_{10}O_8 \rightarrow W_2Sn_8S_{10}O_7 + ½O_2\ (\Delta G = 3.855\ \text{eV}), \quad (7)$$

$$W_2Sn_8S_{10}O_8 + ½O_2 \rightarrow W_2Sn_8S_{10}O_9\ (\Delta G = 0.835\ \text{eV}). \quad (8)$$

Comparing Eq. (8) with Eq. (3), oxidizing the $W_2Sn_8S_{10}O_8$ cluster needs approximately half the energy required to oxidize the $Sn_{10}S_{16}$ cluster. The $W_2Sn_8S_{10}O_8$ cluster can adsorb NO_2 more efficiently than SnS_2, as in the equation:

$$W_2Sn_8S_{10}O_8 + NO_2 \rightarrow [W_2Sn_8S_{10}O_8...NO_2]^a\ (\Delta G = 0.0656\ \text{eV}). \quad (9)$$

The energy needed for the adsorption of NO_2 on the doped SnS_2 cluster is half of the pristine cluster. Finally, the reaction of the (oxygen-deficient or vacancy) $W_2Sn_8S_{10}O_7$ cluster with NO_2 is more vigorous than the pristine (with sulfur vacancy) SnS_2 (Eqs. (5, 6)) clusters:

$$W_2Sn_8S_{10}O_7 + NO_2 \rightarrow W_2Sn_8S_{10}O_8 + NO\ (\Delta G = -3.420\ \text{eV}), \quad (10)$$

$$[W_2Sn_8S_{10}O_8...NO_2]^a + W_2Sn_8S_{10}O_7 \rightarrow 2W_2Sn_8S_{10}O_8 + NO\ (\Delta G = -3.485\ \text{eV}). \quad (11)$$

Several parameters are needed to apply the TST to evaluate the reaction rate of pristine and WO_3-doped SnS_2 clusters with NO_2 gas. The TST formula for the reaction rate of $W_2Sn_8S_{10}O_7$ clusters (with a vacancy) with NO_2 can be given by [24]:

$$\frac{d[W_2Sn_8S_{10}O_7]}{dt} = -[W_2Sn_8S_{10}O_7]^u [NO_2]_e^v k(T), \quad (12)$$

$$k(T) = AT^m \exp^{\left(\frac{-\Delta G^{\ddagger}}{k_B T}\right)}. \quad (13)$$

In Eqs. (12, 13), $[W_2Sn_8S_{10}O_7]$ and $[NO_2]$ are the concentration of doped sensor clusters and the concentration of NO_2 gas, respectively. (u and v) are concentration exponents that can be determined from experimental data. (u and v) have a value of 1, which is also the value of some previous TST sensor calculations [25]. $k(T)$ in Eqs. (12, 13) is the temperature-dependent part of the reaction rate. (A) is an experimental parameter that considers the sensor materials properties such as morphology, crystallinity, surface structure, and manufacturing methods. (m) The temperature exponent in Eq. (13) is a parameter that can be determined experimentally from the response variation with gas sensor temperature. $\Delta G^{\ddagger}$ is the Gibbs energy of transition (or activation), and k_B is the Boltzmann constant. The subscript (e) in the NO_2 gas concentration is the effect of dissociation on NO_2 concentration in Eq. (1) as given by the equation:

$$[NO_2]_d = \frac{[NO_2]}{1 + e^{k_s(T - T_0)}}, \quad (14)$$

$$[NO_2]_e = [NO_2] - \frac{[NO_2]}{1 + e^{k_s(T - T_0)}}. \quad (15)$$

In the above equations, $[NO_2]_d$ and $[NO_2]_e$ are the dissociated and effective NO_2 gas concentrations. k_s is the rate at which NO_2 dissociates, while T_0 is the temperature at which NO_2 concentration reaches half its original concentration. Eqs. (14, 15) does not take humidity effect into account. To consider humidity effects, Eq. (15) is modified to:

$$[NO_2]_e = [NO_2] - \frac{[NO_2]}{1 + e^{k_s(T - T_0)}} \frac{1}{1 + e^{k_h(h - h_0)}}. \quad (16)$$

In the above equation, h is the relative humidity, k_h is the rate at which NO_2 effective concentration decreases due to humidity, and h_0 is the humidity at which NO_2 concentration reaches half of its concentration due to humidity.

Changing Eq. (12) to a difference equation, the number of clusters with a vacancy ($W_2Sn_8S_{10}O_7$) that changes to a stable cluster ($W_2Sn_8S_{10}O_8$) per unit of time can be given by:

$$\Delta\left[W_2Sn_8S_{10}O_8\right] = -\Delta\left[W_2Sn_8S_{10}O_7\right] = \left[NO_2\right]_e^v k(T)\left[W_2Sn_8S_{10}O_7\right]^u \Delta t. \quad (17)$$

The negative sign is added since the decrease of vacancies ($W_2Sn_8S_{10}O_7$) is an increase in fully oxidized clusters ($W_2Sn_8S_{10}O_8$). Using the above equation and assuming that the total number of $W_2Sn_8S_{10}O_7$ clusters is nearly constant (not changing appreciably), the response can be given by:

$$\text{Response}(\text{theoretical}) = 1 + c[NO_2]_e^v \; k(T). \quad (18)$$

In Eq. (18), (c) is an experimental factor that correlates the change in the number of vacancies to the change in response, including the effective time (Δt) needed to oxidize these vacancies. The theoretical response is compared to the measured experimental response given by the ratio (R_g/R_a). R_g is the sensor resistance when the NO_2 gas mixed with air passes over the sensor surface, and R_a is the resistance when pure air passes over the sensor surface. Both theoretical and experimental responses reduce to 1 when the NO_2 gas concentration vanishes ($R_g = R_a$). This ratio (R_g/R_a) is the reciprocal of response to reducing gases (R_a/R_g).

Results and Discussion

Figure 1 shows the adsorption and transition states of the NO_2 gas molecule on the surface of the $W_2Sn_8S_{10}O_8$ cluster. In the adsorption case, the negative charges in NO_2 are attracted to positive charges in the sensor cluster, and the positive charges in NO_2 are attracted to negative charges in the sensor cluster. Using NBO (natural bond order) analysis, N and O atoms in NO_2 have the charges 0.514 and –0.257 electronic charges, respectively. The Sn and S atoms in the pristine sensor mostly have 1.4 and –0.8 electronic charges, respectively. The same is true in the WO_3 doped cluster in which Sn and W have positive charges, and S and O have negative electronic charges. In the transition state case, the positive charges of the gas are nearer to the positive charges in the sensor, and the negative charges of the gas are closer to the negative charges in the sensor, resulting in higher energy. The calculated bond length of Sn–S is around 2.6 Å, which is in good agreement with previous experimental and theoretical values [26]. The W–O bond length is 1.7–1.85 Å, which agrees with previous experimental and theoretical results [27]. The calculated HOMO-LUMO gap is 3.076 eV compared to experimental 2.34–2.42 eV [28]. Being larger than the experimental value is expected because of the theoretical cluster's SnS_2 cluster size (or the number of atoms). After doping with WO_3, the HOMO-LUMO gap is 2.417 eV.

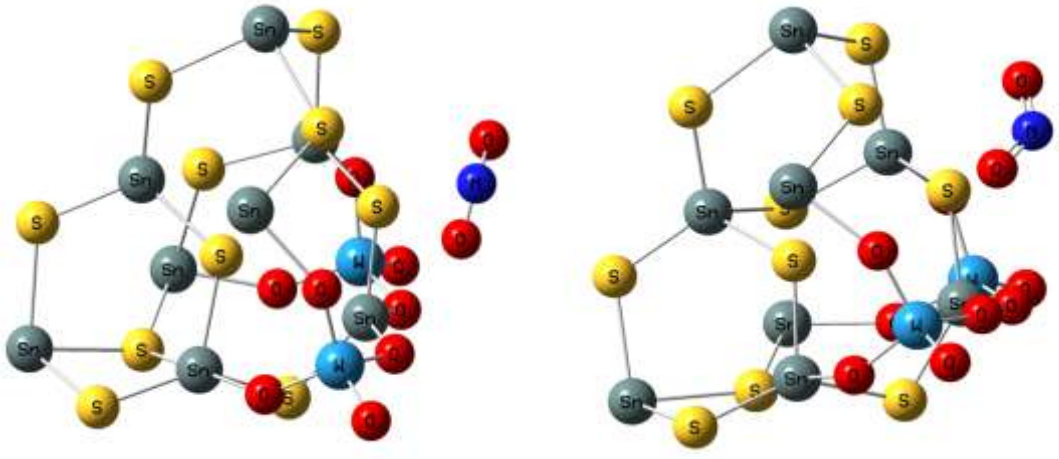

a *b*

Figure 1. (*a*) Optimization of NO_2 adsorption on $W_2Sn_8S_{10}O_8$ cluster and (*b*) the optimization of NO_2 transition state on $W_2Sn_8S_{10}O_8$ surface cluster

Figure 2 shows the Gibbs free energy of transition as a function of doping (molar) percentage and temperature. The experimental lowest percentage of doping at 30 % molar is near the theoretically lowest determined Gibbs free energy of transition at 25 %. The pristine SnS_2 (zero doping percentage) sensor has very high Gibbs energy compared to doped clusters at all shown temperature ranges. The Gibbs free energy of

transition for various percentages can be calculated using the modified Evans–Polanyi principle by interpolation [29]:

$$\Delta G^{\ddagger} = \Delta G_0^{\ddagger} + \beta \Delta G_1^{\ddagger} \tag{19}$$

In Eq. (19), $\Delta G_0{}^{\ddagger}$ and $\Delta G_1{}^{\ddagger}$ are known Gibbs free energy of transition values for two different percentages, and β is the interpolation coefficient. The Gibbs free energy of transition is the sum of two terms, enthalpy ($\Delta H^{\ddagger}$) and entropy ($\Delta S^{\ddagger}$) of transition:

$$\Delta G^{\ddagger} = \Delta H^{\ddagger} - T\Delta S^{\ddagger} \tag{20}$$

After doping, transition entropy increases, leading to a lower transition energy, as in Eq. (20).

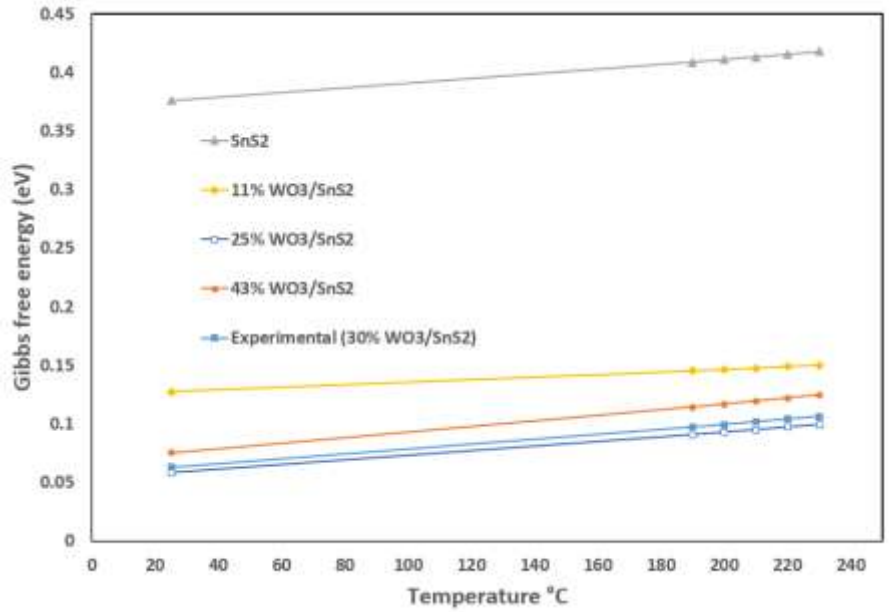

Figure 2. Gibbs energy of transition or activation of NO_2 with pristine and WO_3 doped SnS_2 as a function of temperature for different molar percentages of the doping material WO_3

Table 1 shows the parameters that are used in the present calculations. The parameters are for the 30 % WO_3 doped SnS_2 cluster reaction with NO_2 gas. The adsorption state is designated as [30 %WO_3/SnS_2 --- NO_2]^a, while the transition state is designated as [30 %WO_3/SnS_2 --- NO_2]‡. The experimental response for the 30 % WO_3 doped SnS_2 to NO_2 gas is available [3]. The Gibbs free energy of transition ($\Delta G^{\ddagger}$) is calculated using the Gaussian 09 method (*ts*) as in the optimization statement (OPT=(calcfc, ts, noeigen)) to calculate the transition state. The value of $\Delta G^{\ddagger}$ for the 30 % WO_3 doped SnS_2 cluster is 0.0629 compared to 0.376 eV for the pristine SnS_2 cluster, which is six times lower.

Table 1

Reaction parameters of 30 % WO_3 doped SnS_2 to NO_2 gas. $\Delta G^{\ddagger}$ value is at 25 °C and 1 bar

Reaction	$\Delta G^{\ddagger}$ (eV)	A (s^{-1}. K^{-12})	m	v, u	k_s ($°C^{-1}$)	T_0 (°C)	k_h		h_0 (%)	c (s)
[30 %WO_3/SnS_2 --- NO_2]^a ↓ [30 % WO_3/SnS_2 --- NO_2]‡	0.0629	2.8×10^{-28}	12	1	0.15	220	0.11		100	880

The (A) parameter reflects the sensor material's manufacturing method and materials properties. The properties of the materials include surface area, crystallinity, doping, electronic structure, etc. The units of this parameter are affected by the temperature exponent (m) and the correlation parameter (c).

The temperature exponent (m) has a value of 12. This high value is also found in other materials' response to NO_2 gas [30]. The range of m for the reaction of investigated gases with sensor materials is (1 to 12). The high value of m is a sign of a vigorous reaction between NO_2 gas and doped sensor material.

The concentration exponents (u, v) are equal to one (1). These values are the values in the original transition state theory. The u exponent is always taken as one, while the v exponent (gas concentration exponent) can take the range ½ to 2 depending on the kind of gas or sensor material.

The temperature-dependent logistic function parameters of Eq. (14) are k_s and T_0. These parameters have values of 0.15 °C^{-1} and 220 °C, respectively, as in Table 1. The dissociation rate is higher than the dissociation of NO_2 over other materials [30]. The half concentration temperature T_0 is near the NO_2 dissociation temperature at 200 °C.

The parameters of the humidity-dependent logistic function of Eq. (16) show the usual humidity-dependent NO_2 decrease rate (k_h) value [29]. The humidity at which the effective NO_2 concentration is half its original concentration (T_h) is high at 100 %, reflecting minimal humidity effects on the sensor material. These results show that the sensor material is perfect for decreasing the effect of humidity.

The last parameter is the response correlation parameter (c). The high value of this parameter indicates the high sensitivity and response of the doped material. Comparing the value of this parameter with previous studies for various materials and doping reveals that the present 30 % WO_3 doped SnS_2 is one of the best materials to detect NO_2 gas [30].

Figure 3 shows a schematic diagram of Gibbs energy of adsorption and transition state of NO_2 with pristine and WO_3 doped SnS_2 at room temperature. The Gibbs energy of the transition state is the highest energy barrier needed to be overcome for the reaction to proceed. As shown in Figure 3, doping SnS_2 with WO_3 can reduce this barrier to more than six times. As a result, the reaction rate increases dramatically after doping.

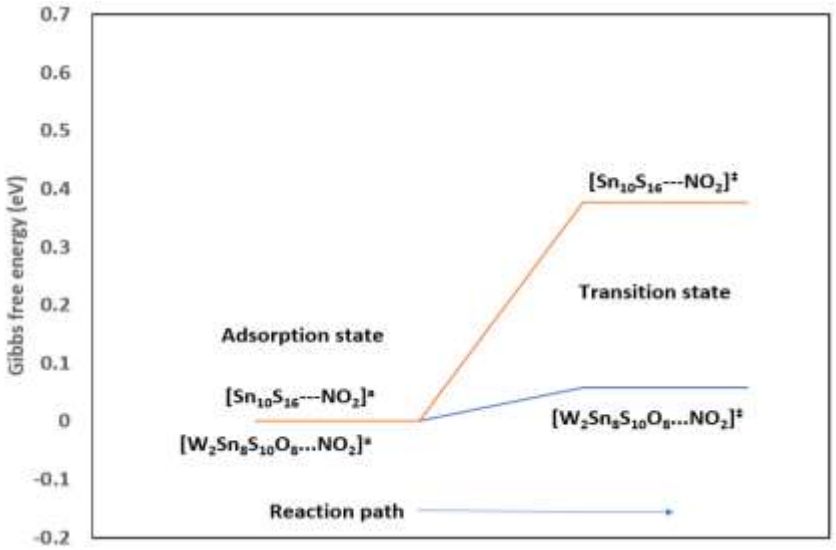

Figure 3. Schematic diagram of Gibbs energy of adsorption and transition state of NO_2 with pristine and 30 % WO_3 doped SnS_2 at room temperature. All energies are taken with reference to adsorption state energy

Figure 4 compares the theoretical response of 30 % WO_3 doped SnS_2 as a function of temperature and experimental results (R_g/R_a) [3] to 20 ppm of NO_2 at low humidity. The comparison shows acceptable results for temperatures higher than 210 °C and less matching for temperatures lower than 210 °C. Both theoretical and experimental results peak at 210 °C; however, experimental results have relatively sharper peak that are less pronounced theoretically.

Figure 5 shows the theoretical response of 30 % WO_3 doped SnS_2 as a function of NO_2 concentration at temperature 210 °C compared with experimental results (R_g/R_a). The linear theoretical response, as established by Eq. (18) (v = 1), is close and generally lower than the experimental values. As the introduction mentions, the detected concentration can be lower than the allowed NO_2 concentration in the range 1–5 ppm range.

Figure 6 shows the 90 % response time to 20 ppm NO_2 of 30 % WO_3 doped SnS_2 as a function of temperature in comparison with experiment [3] at low humidity. The 90 % response time can be obtained by integrating Eq. (12), resulting in the equation:

$$t_{res(90\ \%)} = \frac{\ln(10)}{[NO_2]_e^{v}\, AT^{m}\, \exp\left(\frac{-\Delta G^{\ddagger}}{k_B T}\right)} \tag{21}$$

90 % response time is the duration for a sensor to reach 90 % of its final, stable reading after exposure to the detected gas. A good agreement between theory and experiment is obtained in Figure 6.

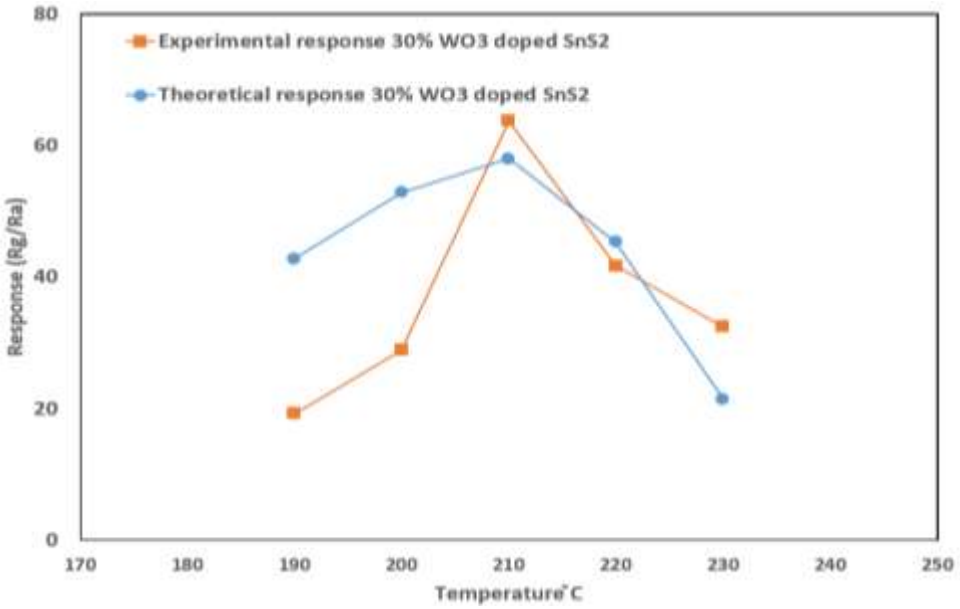

Figure 4. Theoretical response of 30 % WO_3 doped SnS_2 as a function of temperature compared with experimental results (R_g/R_a) [3] to 20 ppm of NO_2 at low humidity

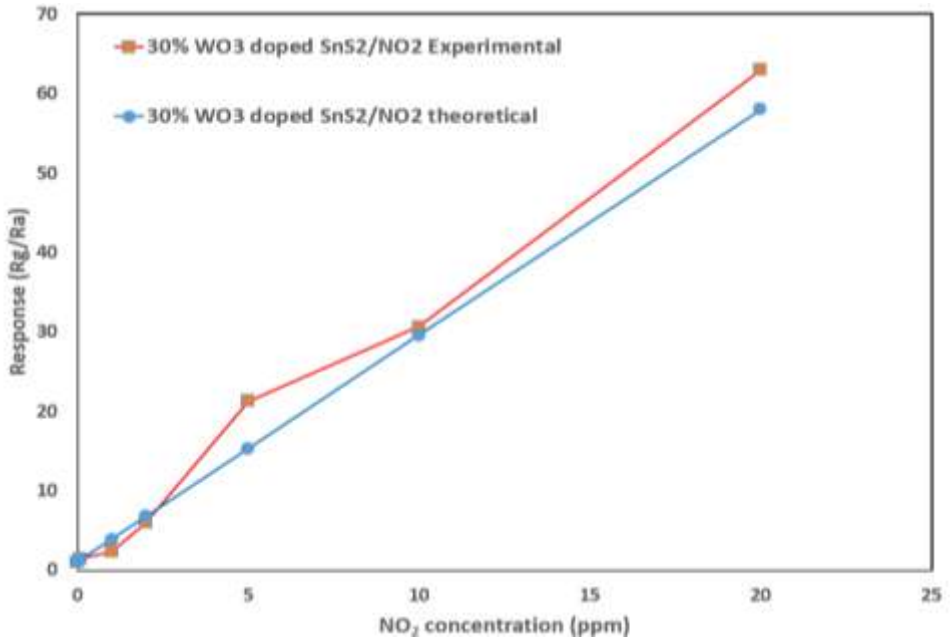

Figure 5. Theoretical response of 30 % WO_3 doped SnS_2 as a function of NO_2 concentration at temperature 210 °C compared with experimental results (R_g/R_a) [3] at low humidity

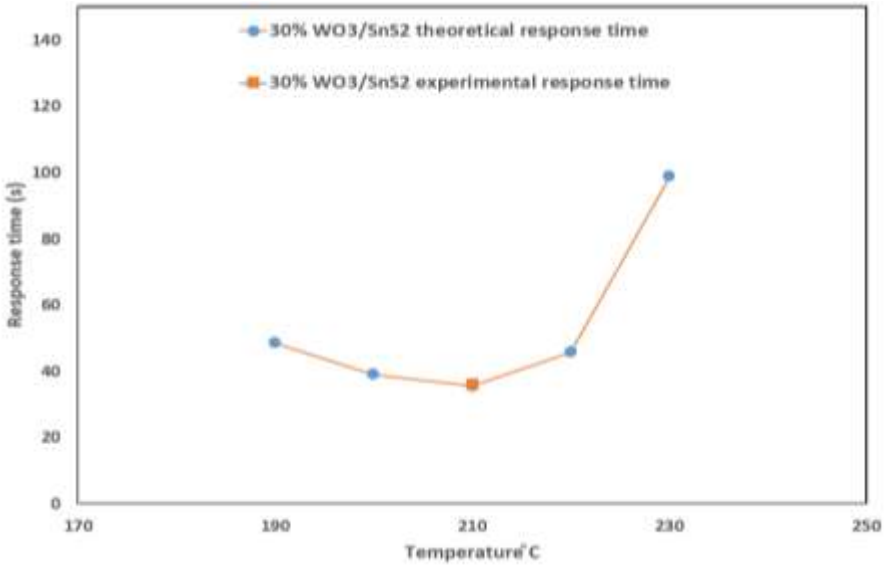

Figure 6. 90 % response time to 20 ppm NO_2 of 30 % WO_3 doped SnS_2 as a function of temperature in comparison with experiment [3] at low humidity

Figure 7 shows the effect of relative humidity on 30 % WO_3 doped SnS_2 response to 20 ppm of NO_2 gas at 210 °C temperature compared with the experiment [3]. Relative humidity affects response mainly in high humidity only, which can also be deduced from humidity parameters in Table 1. This indicates good response at relatively low to medium humidity.

Figure 8 shows the response stability after 30 days of 20 ppm NO_2 of 30 % WO_3 doped SnS_2 at 210 °C temperature compared to the experiment [3]. The theoretical response is equal to or lower than the experimental response, as shown in Figure 5 for higher NO_2 concentrations. As time passes (several months), it is expected for the detected response to be reduced further, and the experimental response becomes nearer to the theoretical response in Figure 8. Material degradation that includes changes in material crystallinity, doping, and electronic structure can all decrease the sensitivity. Dust, temperature fluctuations, and even pressure fluctuations affect sensor readings.

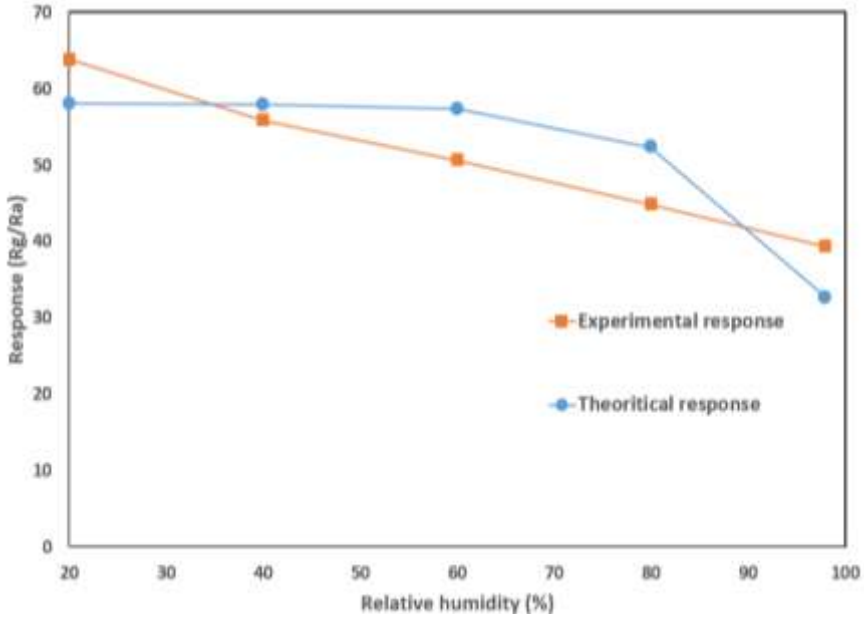

Figure 7. The effect of relative humidity on 30 % WO_3 doped SnS_2 response to 20 ppm of NO_2 gas at 210 °C temperature compared with experiment [3]

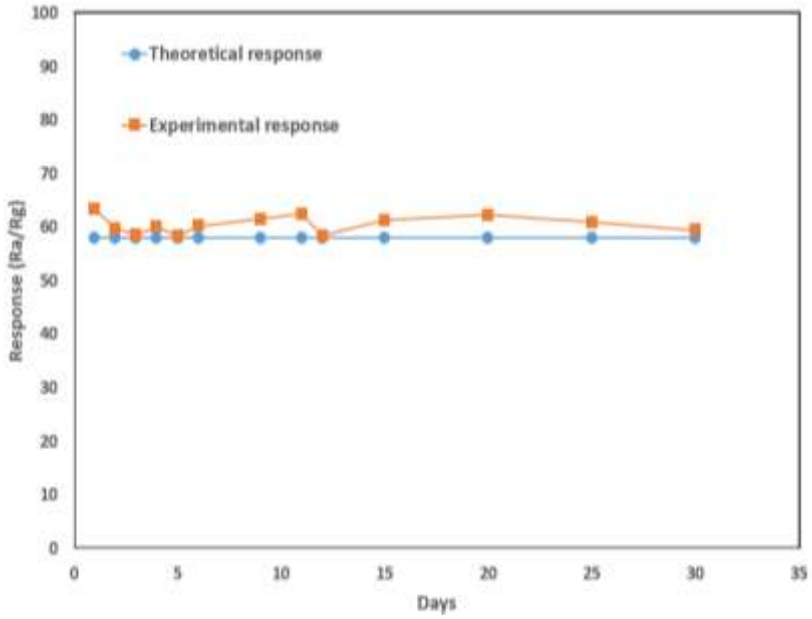

Figure 8. The stability of response after 30 days of 20 ppm NO_2 of 30 % WO_3 doped SnS_2 at 210 °C temperature compared to experiment [3]

Figure 9 summarizes the NO_2 dissociation in air and reaction with the sensor material.

As the NO_2 molecule approaches the sensor material, its temperature rises to reach the sensor temperature (210 °C for the present sensor). NO_2 begins to dissociate as it passes its dissociation temperature. Other NO_2 molecules that reach the sensor material might get adsorbed. Some of the NO_2-adsorbed molecules might oxidize an oxygen vacancy in the sensor material, increasing the sensor's resistance and getting detected by the electronic circuit connected to the sensor material.

The present theoretical method adds new methods to distinguish between detected gases and response values at a given temperature [3]. The distinguishing method depends on the temperature at which the detected gas dissociates (such as NO_2 in the present work at 200 °C) or reaches its autoignition temperature such as ethanol at 368 °C [24]. After the dissociation or autoignition temperatures, the gas concentration and response drop rapidly. Scanning the temperature-response profile of a detected gas can add information that differentiates between several gases.

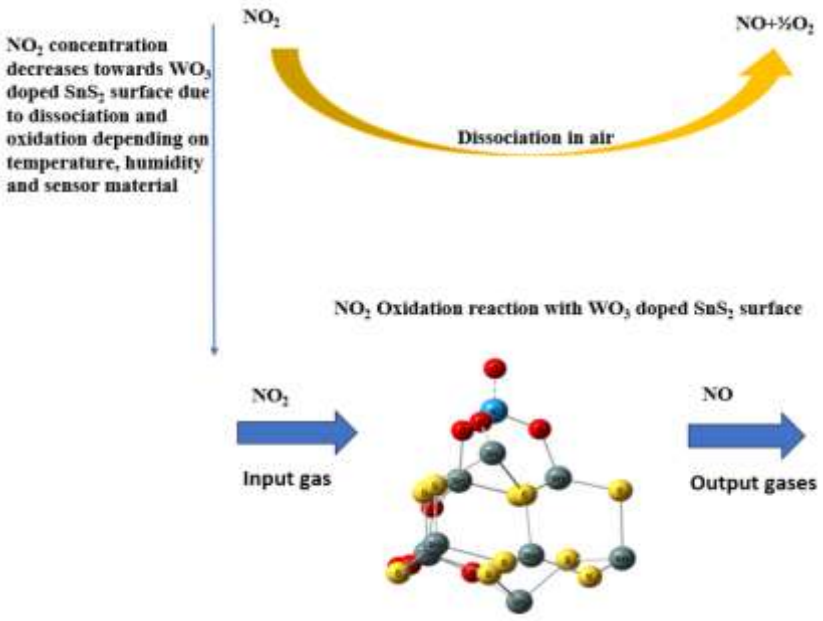

Figure 9. Summarizing the NO_2 dissociation in air and reactions with the sensor material

Conclusions

The reaction rate equation in transition state theory was used to evaluate the change in the number of vacancies in a 30 % WO_3 doped SnS_2 sensor as NO_2 gas passes over its surface. The change in number of vacancies was correlated to the change in response and response time. The Gibbs free energy of transition was evaluated to calculate the change of response with temperature and gas concentration. Gibbs free energy of transition showed low values of activation barrier near the highest response of experimentally determined doping ratio, indicating the quality of the used theory. The calculated response variation with temperature and NO_2 concentration agrees with the experimental response (R_g/R_a) variation. The response time is also in good agreement with the experiment. The effect of humidity was also considered and compared to the experiment. The sensor material shows good stability for long-term use and nearly stays around a specific value with some fluctuations for a month. The present theory can distinguish different gases by the gas properties, such as dissociation temperature for NO_2 gas or autoignition temperature for other gases. The use of reaction rate methods such as the TST in the present work is the only available method in literature to simultaneously calculate response, response time, temperature effect, and humidity effect.

*Author Information**

**The authors' names are presented in the following order: First Name, Middle Name and Last Name*

Mudar Ahmed Abdulsattar — Chief Scientific Researcher, Head of Solid-State Department, Ministry of Science and Technology, Rusafa Street, 52, 10045, Baghdad, Iraq, e-mail: mudarahmed3@yahoo.com; https://orcid.org/0000-0001-8234-6686

Author Contributions

The manuscript was written through contributions of all authors. All authors have given approval to the final version of the manuscript. CRediT: **Mudar Ahmed Abdulsattar** — supervision, data curation, methodology, review & editing.

Conflicts of Interest

The authors declare no conflict of interest.

References

1 Lin, G., Zheng, T., Zhan, L., Lu, J., Huang, J., Wang, H., Zhou, Y., Zhang, X., & Cai, W. (2020). Tunable Structure and Optical Properties of Single Crystal SnS_2 Flakes. *Applied Physics Express*, *13*. https://doi.org/10.35848/1882-0786/ab7443

2 Zhang, L., Xu, J., Lei, X., Sun, H., Ai, T., Ma, F., & Chu, P.K. (2025). Edge-Enriched SnS_2 Nanosheets on Graphene for Chemiresistive Room Temperature NH_3 Sensors. *Sensors and Actuators B: Chemical*, *433*. https://doi.org/10.1016/j.snb.2025.137565

3 Zhao, H., Lv, J., Ma, X., Huang, B., Han, L., Kang, X., Wang, D., & Fang, H. (2025). Highly Responsive WO_3/SnS_2 Sensor with Humidity Compensation: NO_2 Real-Time Detection System in Soil Surface Layer. *Sensors and Actuators B: Chemical*, *429*. https://doi.org/10.1016/j.snb.2025.137318

4 Lee, S.M., Kim, Y.J., Park, S.J., Cheon, W.S., Kim, J., Nam, G.B., Kim, Y., & Jang, H.W. (2025). In-Situ Growth of 2D MOFs as a Molecular Sieving Layer on SnS_2 Nanoflakes for Realizing Ultraselective H_2S Detection. *Advanced Functional Materials*, *35*. https://doi.org/10.1002/adfm.202417019

5 Wang, Y., Li, J., Zhang, D., Zhou, T., Sun, M., Chen, S., & Sun, M. (2025). Hydrothermal Synthesis of Ag-Doped WO_3-Based H_2S Room Temperature Sensors: Unprecedented High and Fast Response. *Sensors and Actuators B: Chemical*, *438*. https://doi.org/10.1016/j.snb.2025.137811

6 Liaqat, M.J., Hussain, S., Shahid, A., Amu-Darko, J.N.O., Ibrahim, T.K., Ibrahim, S.M., Manavalan, R.K., Zhang, X., Qiao, G., & Liu, G. (2025). Hydrothermally Grown WO_3-SnO_2 Nanocomposites for Efficient NO_2 Detection at Low Concentration. *Sensors and Actuators B: Chemical*, *436*. https://doi.org/10.1016/j.snb.2025.137711

7 An, B., Yang, Y., Yan, J., Wang, Y., Li, R., Wu, Z., Zhang, T., Han, R., Cheng, X., Wang, Q., & Xie, E. (2025). Oxygen Vacancies Engineering and Palladium Quantum Dots Sensitized WO_3 Nanosheet for Highly Efficiently H_2 Detection. *Applied Surface Science*, *692*. https://doi.org/10.1016/j.apsusc.2025.162722

8 Airgas. (2018). Safety Data Sheet Nitrogen Dioxide (NO_2). Pennsylvania. chrome-extension://efaidnbmnnnibpcajpcglclefindmkaj/https://www.airgas.com/msds/001041.pdf

9 Chen, X., Chen, X., Han, Y., Su, C., Zeng, M., Hu, N., Su, Y., Zhou, Z., Wei, H., & Yang, Z. (2019). Two-Dimensional $MoSe_2$ Nanosheets via Liquid-Phase Exfoliation for High-Performance Room Temperature NO_2 Gas Sensors. *Nanotechnology*, *30*. https://doi.org/10.1088/1361-6528/ab35ec

10 Sobrinho, H.H. de O., Eising, R., & Wrasse, E.O. (2025). Nanomaterials as Medicinal Gas Sensors Described by Density Functional Theory: A Comprehensive Review. *Medical Gas Research*, *15*, 435–441. https://doi.org/10.4103/mgr.MEDGASRES-D-24-00121

11 Abdulsattar, M.A. & Mahmood, T.H. (2023). Enhancement of SnO_2 Sensitivity to Acetone by Au Loading: An Application of Evans–Polanyi Principle in Gas Sensing. *Optik*, *275*, 170604. https://doi.org/10.1016/j.ijleo.2023.170604

12 Abdulsattar, M.A. (2024). Effect of Acetylene Properties on Its Gas Sensing by NiO Doped ZnO Clusters: A Transition State Theory Model. *Eurasian Journal of Chemistry*, *29*, 35–43. https://doi.org/10.31489/2959-0663/4-24-8

13 Abdulsattar, M. A., & Almaroof, S. M. (2025). H_2S Properties and Temperature Effects on the Response of Pristine and Al-Doped ZnO Gas Sensor. *Eurasian Journal of Chemistry*, *30*(1(117)), 40–49. https://doi.org/10.31489/2959-0663/1-25-10

14 Sun, S., Li, X., Wang, N., Huang, B., & Li, X. (2025). A Sensitive Ppb-Level NO_2 Sensor Based on SnO_2 Decorated Te Nanotubes. *Sensors and Actuators B: Chemical*, *428*. https://doi.org/10.1016/j.snb.2025.137238

15 Kim, T., Kim, W., Kim, S., & Lee, W. (2025). Sensitive and Stable NO_2 Sensor in a Wide Range Based on RGO/ZnO via Simple Spray Coating. *Microchemical Journal*, *212*. https://doi.org/10.1016/j.microc.2025.113250

16 Rani, S., Dahiya, R., Kumar, V., Berwal, P., & Sihag, S. (2024). Hydrothermally Engineered WO_3 Nanosheets as Potential NO_2 Gas Sensor. *Ionics*, *31*, 993–1002. https://doi.org/10.1007/s11581-024-05934-2

17 Frisch, M.J., Trucks, G.W., Schlegel, H.B., Scuseria, G.E., Robb, M.A., Cheeseman, J.R., Scalmani, G., Barone, V., Mennucci, B., Petersson, G.A., Nakatsuji, H., Caricato, M., Li, X., Hratchian, H.P., Izmaylov, A.F., Bloino, J., Zheng, G., Sonnenberg, J.L., Hada, M., Ehara, M., Toyota, K., Fukuda, R., Hasegawa, J., Ishida, M., Nakajima, T., Honda, Y., Kitao, O., Nakai, H., Vreven, T., Montgomery, J.A.J., Peralta, J.E., Ogliaro, F., Bearpark, M., Heyd, J.J., Brothers, E., Kudin, K.N., Staroverov, V.N., Kobayashi, R., Normand, J., Raghavachari, K., Rendell, A., Burant, J.C., Iyengar, S.S., Tomasi, J., Cossi, M., Rega, N., Millam, J.M., Klene, M., Knox, J.E., Cross, J.B., Bakken, V., Adamo, C., Jaramillo, J., Gomperts, R., Stratmann, R.E., Yazyev, O., Austin, A.J., Cammi, R., Pomelli, C., Ochterski, J.W., Martin, R.L., Morokuma, K., Zakrzewski, V.G., Voth, G.A., Salvador, P., Dannenberg, J.J., Dapprich, S., Daniels, A.D., Farkas, Ö., Foresman, J.B., Ortiz, J. V., Cioslowski, J., & Fox, D.J. (2013). Gaussian 09, Revision D.01. Gaussian, Inc., Wallingford CT.

18 Cai, J., Hao, S., Zhang, Y., Wu, X., Li, Z., & Zhao, H. (2024). Co_3O_4 as an Efficient Passive NO_x Adsorber for Emission Control during Cold-Start of Diesel Engines. *Chinese Journal of Chemical Engineering*, *66*, 1–7. https://doi.org/10.1016/j.cjche.2023.10.013

19 Abdulsattar, M.A. (2024). NO_2 Properties That Affect Its Reaction with Pristine and Pt-Doped SnS_2: A Gas Sensor Study. *Journal of Molecular Modeling*, *30*. https://doi.org/10.1007/s00894-024-06223-5

20 Ambi, R.R., Mali, R.A., Pawar, A.B., Mulla, M.M., & Pittala, R.K. (2025). NiO Nanosheet-Assembled Chemiresistive Sensor for NO_2 Detection. *Applied Physics A: Materials Science and Processing*, *131*. https://doi.org/10.1007/s00339-025-08320-5

21 Nikam, S.M., Patil, T.S., Nimbalkar, N.A., Kothavale, V.P., Kamble, R.S., Gaikwad, G.A., Mane, S.M., Lee, J., & Mane, R.D. (2025). Nickel Ion-Doped Vertical Nanorod Array Network of ZnO Engineered by Chemical Bath Deposition for Versatile NO_2 Gas Sensor. *Journal of the Korean Ceramic Society*, *62*, 330–349. https://doi.org/10.1007/s43207-024-00469-8

22 Hu, Y., Chen, T., Wang, X., Ma, L., Chen, R., Zhu, H., Yuan, X., Yan, C., Zhu, G., Lv, H., Liang, J., Jin, Z., & Liu, J. (2017). Controlled Growth and Photoconductive Properties of Hexagonal SnS2 Nanoflakes with Mesa-Shaped Atomic Steps. *Nano Research*, *10*, 1434–1447. https://doi.org/10.1007/s12274-017-1525-3

23 Wang, M., Chen, J., Zhang, C., Ding, H., Wu, H.H., Li, X., Huai, S., Tang, Z., Zhao, X., Liu, H., & Wang, X. (2025). Engineering Surface Defect Active Sites in SnS_2 Nanosheets with Electron-Donating Groups for Efficient Photoelectrochemical Water Splitting. *Journal of Catalysis*, *446*. https://doi.org/10.1016/j.jcat.2025.116087

24 Abdulsattar, M.A., Jabbar, R.H., & Al-Seady, M.A. (2024). Ethanol Properties Effects on Its Reaction with Mo-Doped SnO_2 Clusters: A Gas Sensor Model. *Results in Surfaces and Interfaces*, *17*. https://doi.org/10.1016/j.rsurfi.2024.100291

25 Abdulsattar, M.A., Jabbar, R.H., Abed, H.H., & Abduljalil, H.M. (2021). The Sensitivity of Pristine and Pt Doped ZnO Nanoclusters to NH_3 Gas: A Transition State Theory Study. *Optik*, *242*. https://doi.org/10.1016/j.ijleo.2021.167158

26 Khan, W., & Reshak, A.H. (2015). Electronic Properties of Orthorhombic BaSn2S5 Single Crystal. *Indian Journal of Physics*, *89*, 437–443. https://doi.org/10.1007/s12648-014-0605-4

27 Zhang, B.F., Lin, J.Z., Wang, Y.X., Zhao, Y., & Zhang, Y.F. (2023). Theoretical Studies on the G-Factors and the Local Structure of W^{5+} Ions in Tungsten Phosphate Glasses. *Revista Mexicana de Fisica*, *69*. https://doi.org/10.31349/RevMexFis.69.040402

28 Sawini, Singh, K., Kumar, A., Kumar, D., Kumar, A., Kumar, A., Mahatha, S.K., & Praveenkumar, S. (2025). Unveiling the Role of Temperature on Structural, Compositional, Morphological, Thermal and Optical Properties of Hydrothermally Synthesized SnS_2 Nanostructures. *Inorganic Chemistry Communications*, *171*. https://doi.org/10.1016/j.inoche.2024.113548

29 Abdulsattar, M.A., Almaroof, H.M., & Al-Saraf, W.J. (2025). Cl_2 Gas Properties, Temperature, and Humidity Effects on SnO_2 Sensor Response: Transition State Theory Study. *Journal of Molecular Modeling*, *31*. https://doi.org/10.1007/s00894-025-06368-x

30 Abdulsattar, M.A. (2025). Pristine and Ni-Doped In_2O_3 Pyramids Response to NO_2 Gas: A Transition State Theory Study. *Interactions*, *246*. https://doi.org/10.1007/s10751-025-02282-z